Global and Planetary Change 129 (2015) 10–22

Contents lists available at ScienceDirect

Global and Planetary Change

journal homepage: www.elsevier.com/locate/gloplacha

Impacts, effectiveness and regional inequalities of the GeoMIP *G1* to *G4* solar radiation management scenarios

Xiaoyong Yu [a,b], John C. Moore [a], Xuefeng Cui [a,*], Annette Rinke [c], Duoying Ji [a], Ben Kravitz [d], Jin-Ho Yoon [d]

[a] State Key Laboratory of Earth Surface Processes and Resource Ecology, College of Global Change and Earth System Science, Beijing Normal University, Beijing 100875, China
[b] Department of Geography, Cambridge University, Cambridge CB2 3EN, UK
[c] Alfred Wegener Institute Helmholtz Centre for Polar and Marine Research, Telegrafenberg A43, 14473 Potsdam, Germany
[d] Atmospheric Sciences and Global Change Division, Pacific Northwest National Laboratory, Richland, WA 99354, USA

ARTICLE INFO

Article history:
Received 28 March 2014
Received in revised form 2 September 2014
Accepted 24 February 2015
Available online 4 March 2015

Keywords:
Solar radiation management
Regional inequality
Regional climate compensation effectiveness
GeoMIP

ABSTRACT

We evaluate the effectiveness and the regional inequalities of solar radiation management (SRM) in compensating for simultaneous changes in temperature and precipitation caused by increased greenhouse gas concentrations. We analyze the results from Earth System Models under four Geoengineering Model Intercomparison Project (GeoMIP) experiments with a modified form of the Residual Climate Response approach. Each experiment produces 50 model yrs of simulations: 13 models completed experiment *G1* (offsetting $4 \times CO_2$ via solar reduction); 12 models completed experiment *G2* (offsetting CO_2 that increased by 1% per year); 3 models completed experiment *G3* (offsetting increasing radiative forcing under RCP4.5 with increasing stratospheric aerosol); and 7 models completed experiment *G4* (injection of 5 Tg SO_2 a^{-1} into the stratosphere). The regional inequalities in temperature and precipitation compensation for experiments *G1*, *G3* and *G4* are significantly different from their corresponding noise backgrounds for most models, but for *G2* they are not significantly different from noise. Differences in the regional inequalities and the actual effectiveness among the four SRM scenarios are not significant for many models. However, in more than half of the models, the effectiveness for temperature in the solar dimming geoengineering scenarios (*G1* and *G2*) is significantly higher than that in the SO_2 geoengineering scenarios (*G3* and *G4*). The effectiveness of the four SRM experiments in compensating for temperature change is considerably higher than for precipitation. The methodology used highlights that a large across-model variation in the treatment of key geoengineering processes (such as stratospheric aerosols) and the quantification of damage caused by climate change creates significant uncertainties in any strategies to achieve optimal compensation effectiveness across different regions.

1. Introduction

Frustrated by the slow progress in carbon dioxide emission reduction, increasing numbers of scientists, politicians and members of the general public are devoting attention to geoengineering, a set of technologies designed to counteract anthropogenic climate change (e.g., Crutzen, 2006; Wigley, 2006; Shepherd et al., 2009; Caldeira and Keith, 2010). Solar radiation management (SRM) is a category of geoengineering that aims to block some solar radiation from reaching the Earth's surface, e.g., by space mirrors in orbit (Mautner, 1989), stratospheric aerosol injection (e.g., Budyko, 1977; Crutzen, 2006) or marine cloud seeding (e.g., Latham, 1990).

Many previous studies of SRM used single models (e.g., Bala et al., 2008; Ricke et al., 2010; MacCracken et al., 2012; Fyfe et al., 2013). As such, determining the modeled impacts and side effects of SRM on the Earth's climate system at global and regional scales is confounded by questions of model dependence of the results. Rasch et al. (2008) compared the results from two models that simulated stratospheric sulfate aerosol injection, but the experiments performed with these models were not consistent, hence difficulties remained in interpreting aerosol effects. Jones et al. (2010) compared the responses of two models to the continuous injection of SO_2 into the lower stratosphere at the rate of 5 Tg a^{-1}, an experiment very similar to GeoMIP experiment *G4* described below. Although there were some similarities in temperature and precipitation response in these two models, their substantial differences prevented the authors from making robust conclusions about the modeled effects of stratospheric sulfate aerosol geoengineering.

To coordinate model simulations of SRM and determine the robust features of climate models to reduced shortwave radiative forcing or sustained layers of stratospheric aerosol, the Geoengineering Model Comparison Project (GeoMIP) was established (Kravitz et al., 2011; see also Fig. 1 for a graphical description of the four core experiments).

* Corresponding author at: College of Global Change and Earth System Science Beijing Normal University, 19 Xinjiekou Wai Street, Beijing 100875, China. Tel.: +86 13681113976.
E-mail address: xuefeng.cui@bnu.edu.cn (X. Cui).

http://dx.doi.org/10.1016/j.gloplacha.2015.02.010
0921-8181/

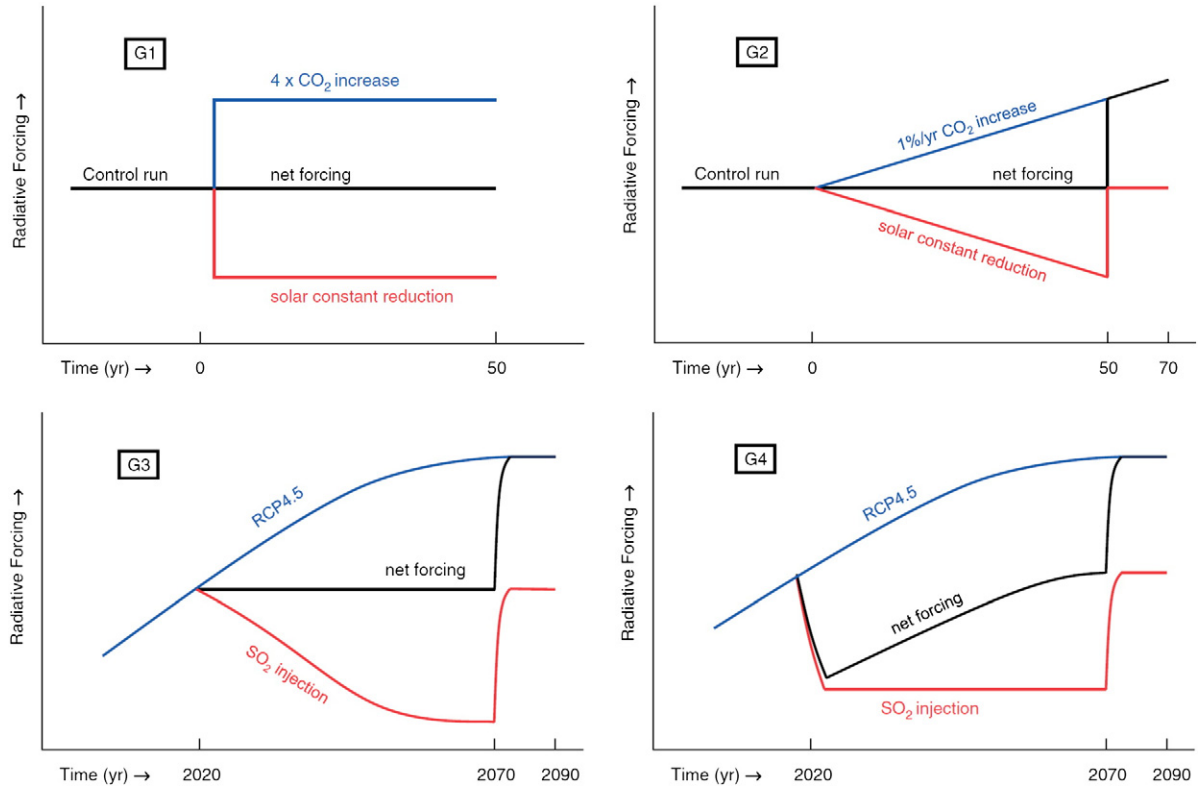

Fig. 1. GeoMIP *G1* to *G4* schemes (reprinted from Kravitz et al., 2011). *G1* is started from a control run. The instantaneous quadrupling of CO_2 concentration from pre-industrial levels is balanced by a reduction in the solar constant until year 50. *G2* also started from a control run. The positive radiative forcing of an increase in CO_2 concentration of 1% per year is balanced by a decrease in the solar constant until year 50. *G3* approximately balances the positive radiative forcing from the RCP4.5 scenario by an injection of SO_2 or sulfate aerosols into the tropical lower stratosphere from year 2020 to year 2069. *G4* experiment is based on the RCP4.5 scenario, where immediate negative radiative forcing is produced by an injection of SO_2 into the tropical lower stratosphere at a rate of 5 Tg yr^{-1} from year 2020 to year 2069.

Several studies have investigated the climate responses to the GeoMIP *G1* (e.g., Schmidt et al., 2012; Kravitz et al., 2013a,b; Tilmes et al., 2013) and *G2* (Jones et al., 2013) experiments. These studies showed a regionally diverse impact on temperature and precipitation, with considerable agreement between models on broad features, such as a warming of the polar regions and cooling of the tropics relative to pre-industrial norms. Kravitz et al. (2014) explored the regional inequalities and effectiveness of global uniform SRM based on *G1* multi-model results. GeoMIP studies of particular regions have thus far only focused on the Arctic responses under *G1* (Moore et al., 2014), *G3* and *G4* experiments (Berdahl et al., 2014).

In this paper, we (1) examine the robustness of modeled global and regional temperature and precipitation responses in the four core GeoMIP experiments and (2) use the residual climate response (RCR) methodology (Moreno-Cruz et al., 2012; discussed in Section 2.3 below) to evaluate climate change compensation effectiveness and regional inequalities of temperature and precipitation in different SRM experiments. The RCR methodology allows for a simple quantitative comparison of different GeoMIP experiments, as it normalizes model results across all of the various experiments and summarizes, as a resultant vector, the net climate response of each climate variable irrespective of the numbers of models running each experiment. This allows us to assess the effectiveness of different types of geoengineering for compensating CO_2 increases. The structure of this paper is as follows: Section 2 describes the four GeoMIP experiments used in this study, as well as the data processing methods; Section 3 discusses global and regional temperature and precipitation changes, regional inequalities and the effectiveness of geoengineering in compensating for changes from CO_2 increases; finally, Section 4 provides a discussion of these results and their implications.

2. Data and analysis methods

2.1. GeoMIP experiment and model description

Among the four standard GeoMIP experiments, *G1* and *G2* are both designed to simulate reduced shortwave radiative forcing by decreasing solar irradiance, while *G3* and *G4* reduce net radiative forcing via the addition of sulfate aerosol precursors to the stratosphere. Experiment *G1* balances an instantaneous increase in CO_2 four times that of pre-industrial levels with a simultaneous solar irradiance reduction. The global mean top-of-atmosphere (TOA) radiation imbalance is specified to be within 0.1 W/m^2 relative to the pre-industrial control simulation for the 50-year experiment (Fig. 1). Experiment *G2* is designed to balance a transient CO_2 increase (1% per year increase in concentration) from pre-industrial levels by gradually decreasing solar irradiance during the first 50 yrs of the experiment; after this period, SRM is switched off while CO_2 continues to increase at the rate of 1% per year for 20 yrs (Fig. 1). For comparison purposes, we also make use of three simulation results from CMIP5 (Taylor et al., 2012) that serve as the background greenhouse gas simulations for experiments *G1* and *G2*: *piControl*, which refers to the pre-industrial control run; *abrupt4xCO2*, which refers to the instantaneous quadrupling of CO_2 from pre-industrial levels; and *1pctCO2*, which refers to 1% per year CO_2 increase from pre-industrial levels.

Unlike *G1* and *G2*, *G3* and *G4* are designed to reduce solar irradiance by stratospheric SO_2 injection (Fig. 1). Over the 50 yrs of *G3*, the injected SO_2 mass is gradually increased to counteract the gradually increased longwave radiative forcing specified under the RCP4.5 scenario, thus maintaining top-of-atmosphere net radiative flux at 2020 levels. In *G4*, the annual amount of SO_2 injected into

the stratosphere is a constant 5 Tg per year for the first 50 yrs of *G4*. *G3* and *G4* do not specify how the models handle aerosols, and the models differ widely in their representations of stratospheric chemistry, aerosol growth and dynamical transport schemes. Thus, it is expected that inter-model differences will be larger for *G3* and *G4* than *G1* and *G2* (Kravitz et al., 2011). The CMIP5 experiment *rcp45*, which is the future climate state forced by RCP4.5 (Taylor et al., 2012), is used for comparison purposes. The baseline climate for *G1*, *G2* and the relevant greenhouse gas forcing experiment is an average of the pre-industrial control simulation *piControl* over time. The RCR vector-based methodology requires a prior state against which comparisons can be made. In the *G3* and *G4* cases, this prior state cannot be simply the mean of *piControl* because the RCP4.5 climate forcing continues from the historical forcing record, which has been non-stationary. Therefore, we chose the average climate under *rcp45* over the period 2010–2029 as the baseline for *G3*, *G4*, and *rcp45* (see Table 1).

During the first few years of all experiments, the short-term feedbacks and transient climate responses will evolve as the models adjust to the new imposed forcings. Therefore, all results reported here are averages over the years 11–50 of the simulations. We recognize that excluding only the first decade is insufficient to isolate the transient response from the steady state response, especially in the *abrupt4xCO2* case, which imposes very large instantaneous changes in radiative forcing. This is a compromise between including enough years of simulation to obtain useful statistics regarding the climate response while excluding some of the more severe transient changes in the climate. Excluding the first decade is consistent with several previous GeoMIP studies (e.g., Schmidt et al., 2012; Kravitz et al., 2013a).

Table 1 lists the number of models available for each GeoMIP scenario and its associated background simulation. The names and general description of the models are given in SI Table 1. In this study, with its emphasis on regional variations, we focus on two important climate variables: near surface air temperature (SAT) and precipitation, as in several previous studies (Ricke et al., 2010; Moreno-Cruz et al., 2012; MacMartin et al., 2013; Ricke et al., 2013; Kravitz et al., 2014).

2.2. Regionalization

We followed Giorgi and Francisco (2000) in defining 22 regions to investigate the patterns of temperature and precipitation change under SRM. These 22 regions cover most of the global land area, and regional boundaries were chosen to represent climatically and physiographically similar land areas. These regions are large enough to produce climate predictions that are more statistically robust than those obtained from grid cell level output (Giorgi and Francisco, 2000; Moreno-Cruz et al., 2012). We calculated the area weighted temperature or precipitation change for each region in each model. The 95% significance level of temperature or precipitation change for each region was also calculated with a two-tailed Student's t-test assuming each model's data was independent.

2.3. Residual climate response method

To evaluate the potential regional inequalities resulting from SRM, as well as the effectiveness of SRM, Moreno-Cruz et al. (2012) introduced the RCR methodology with the objective of providing easily understood results suitable for policy- and decision-makers. In the RCR approach, anthropogenic climate change and the climate change compensated by SRM are represented by two vectors. Each component of these two vectors represents a given region's climate change under greenhouse gas increases or SRM. The angle between these two vectors then represents the difference between the SRM compensated climate and that under the CO_2 equivalent (CO_2e)-driven climate forcing alone.

The prerequisite of applying the RCR method is that regional responses are approximately linear over the forcing range of interest (Moreno-Cruz et al., 2012). Although the climate system is a nonlinear system, and many climate responses are nonlinear, several studies (Ban-Weiss and Caldeira, 2010; Moreno-Cruz et al., 2012; MacMartin et al., 2013) have shown that modeled temperature and precipitation responses over the radiative forcing ranges of their studies are approximately linear with the amount of SRM.

The RCR approach is illustrated in Fig. 2. The origin **O** represents the reference state of a single climate variable **Y** (such as SAT or precipitation, but not a combination of SAT and precipitation as in Moreno-Cruz et al., 2012 and Kravitz et al., 2014; our approach avoids the problem of determining a relative importance among different variables). The regional changes in **Y** from the reference state due to elevated CO_2e are represented as a $1 \times n$ dimension vector $\mathbf{Y}_{CO_2e}$,

$$\mathbf{Y}_{CO_2e} = \left(y_{CO_2e_1}, y_{CO_2e_2}, y_{CO_2e_i}, y_{CO_2e_n}\right) \quad (1)$$

where n is the number of regions in the globe. Each component of $\mathbf{Y}_{CO_2e}$ represents the CO_2e increasing induced **Y** change for a given region $i = 1,2,\ldots n$. The residual change in **Y** under SRM is represented by the vector $\mathbf{Y}_{RES}$,

$$\mathbf{Y}_{RES} = \left(y_{RES_1}, y_{RES_2}, y_{RES_i}, y_{RES_n}\right). \quad (2)$$

In the vector $\mathbf{Y}_{CO_2e}$ and $\mathbf{Y}_{RES}$, the change in **Y** in each region is normalized by the corresponding inter-annual variability of **Y** under the baseline climate, as was done by Ricke et al. (2010). The change compensated by SRM is represented by $\mathbf{Y}_{SRM}$ and is $\mathbf{Y}_{CO_2e} - \mathbf{Y}_{RES}$. The angle φ between $-\mathbf{Y}_{CO_2e}$ and $\mathbf{Y}_{SRM}$ represents the regional inequality in the effectiveness of compensating **Y** change by SRM and is calculated as follows:

$$\varphi = \cos{-1}\left(\frac{-\mathbf{Y}_{CO_2e} \cdot \mathbf{Y}_{SRM}}{\left\|\mathbf{Y}_{CO_2e}\right\| \left\|\mathbf{Y}_{SRM}\right\|}\right). \quad (3)$$

For a non-zero $\mathbf{Y}_{SRM}$, if φ is 0°, all regions are equally compensated by SRM; if φ is 180°, SRM equally increases all regional changes from the

Table 1
Experiments used in this study.

Experiment	Averaging period	Baseline climate	Number of models	
SRM	No SRM			
G1[a]	*abrupt4xCO2*	Experiment year 11–50	Pre-industrial average	13
G2[a]	*1pctCO2*	Experiment year 11–50	Pre-industrial average	12
G3[b]	*rcp45*	Year 2030–2069	Average over 2010–2029 under *rcp45*	3
G4	*rcp45*	Year 2030–2069	Average over 2010–2029 under *rcp45*	7

[a] CESM-CAM5.1-FV was not included in the noise calculation for *G1* and *G2* as its *piControl* simulation only includes model 50 yrs. As a result, the noise calculation involved 12 models in *G1* and 11 models in *G2*.
[b] 4 models in total have completed *G3*, but we exclude GISS-E2-R from the *G3* analysis (see text).

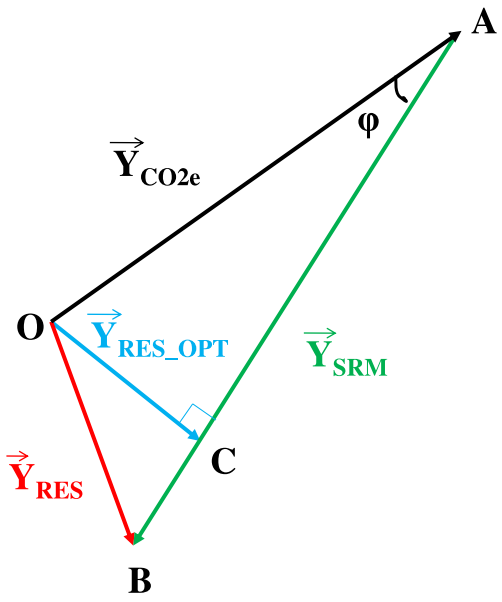

Fig. 2. RCR model illustration. **O** represents the baseline of climate variable **Y**. $\mathbf{Y}_{CO_2e}$ represents the regional changes of climate variable **Y** from the baseline **O** with elevated CO_2e. $\mathbf{Y}_{RES}$ represents the residual change in variable **Y** under SRM. Angle φ represents the regional inequality in the effectiveness of compensating **Y** change by SRM. $\mathbf{Y}_{RES\_OPT}$ represents the optimal residual change for the give angle φ.

elevated CO_2e instead of compensating for them. $\mathbf{Y}_{RES\_OPT}$ is the minimum-norm residual change for a given angle between $\mathbf{Y}_{CO_2e}$ and $\mathbf{Y}_{SRM}$. Geometrically, $\mathbf{Y}_{RES\_OPT}$ is perpendicular to $\mathbf{Y}_{SRM}$ and represents the minimum distance from the baseline to $\mathbf{Y}_{SRM}$. $\mathbf{Y}_{RES\_OPT}$ is assumed to be reached by adjusting the radiative forcing due to SRM equally in all regions. The norm of $\mathbf{Y}_{RES\_OPT}$ depends on φ and the norm of $\mathbf{Y}_{CO_2e}$. A larger φ or norm of $\mathbf{Y}_{CO_2e}$ means a larger norm of $\mathbf{Y}_{RES\_OPT}$.

Following Moreno-Cruz et al. (2012) and MacMartin et al. (2013), we prescribe that regional damages D are a quadratic function of the regional change normalized by the inter-annual variability of the baseline climate, so the damage caused by the change in **Y** could be approximately expressed as follows:

$$D_{CO_2e} \propto \left\|\mathbf{Y}_{CO_2e}\right\|^2 \tag{4}$$

$$D_{RES} \propto \|\mathbf{Y}_{RES}\|^2 \tag{5}$$

$$D_{RES\_OPT} \propto \|\mathbf{Y}_{RES\_OPT}\|^2. \tag{6}$$

The damages caused by climate change are difficult to quantify and we are aware that other damage functional forms have been used in previous studies (e.g., Cline, 1992; Peck and Teisberg, 1992, 1994; Manne et al., 1995). Moreover, there is no indication that a single damage functional form applies equally to all regions or situations. The quadratic function used here is a simple option, but we make no claim that it is more or less valid than other choices.

The percentage of damages compensated by SRM, as calculated from the regional change in the climate variable **Y**, can be represented as:

$$\left(1-\frac{\|\mathbf{Y}_{RES}\|^2}{\left\|\mathbf{Y}_{CO_2e}\right\|^2}\right)\times 100\%. \tag{7}$$

We define the quantity in Eq. (7) to be the actual effectiveness of particular SRM scenario. The optimal effectiveness of a particular SRM scenario for a given φ is then:

$$\left(1-\frac{\|\mathbf{Y}_{RES-OPT}\|^2}{\left\|\mathbf{Y}_{CO_2e}\right\|^2}\right)\times 100\% = \left(1-\sin^2\varphi\right)\times 100\%. \tag{8}$$

An effectiveness of 100% means that the SRM perfectly compensated for all the change in climate variable **Y**; if the effectiveness is negative, then the SRM increased the change in **Y**, rather than compensating for it.

The adjustment percentage of the SRM-compensated change to obtain optimal compensation effectiveness in **Y** is calculated as:

$$\left(\frac{\left\|\mathbf{Y}_{CO_2e}\right\|\cdot\cos(\varphi)}{\|\mathbf{Y}_{SRM}\|}-1\right)\times 100\%. \tag{9}$$

Moreno-Cruz et al. (2012) applied RCR to one geoengineering scenario and for only a single model, whereas here we use RCR to quantify temperature and precipitation compensation effectiveness and regional inequalities in multiple models for four SRM scenarios. Each model's compensation effectiveness and assessments of regional inequalities are taken as independent measurements for the purpose of producing multi-model ensemble means and standard deviations. To investigate the behaviors of φ, actual effectiveness, and optimal effectiveness due to natural variability, we divided the *piControl* runs of each model into several parts, each part containing 40 continuous yrs of simulation. We then can define the first 40 yrs as the 'reference' case and the remainder as 'perfect geoengineering', in which the climate is exactly returned to preindustrial conditions. The differences between the 'perfect geoengineering' and 'reference' climates represent the noise caused by the model's internal variability. We define the 'noise' values of the angle φ, actual effectiveness, and optimal effectiveness from use of the RCR method on these 'perfect geoengineering' periods. Note that the differences between 'perfect geoengineering' and 'reference' in *piControl* may be not a good proxy of natural variability over 2010 to 2029 in RCP4.5, *G3* and *G4*. We use it because there is no obvious way to find the 'perfect geoengineering' for the simulations from 2010 to 2029 in RCP4.5, and similarly for *G3* and *G4*.

The regional inequalities in Kravitz et al. (2014) were demonstrated by regional differences in the path of temperature, precipitation and combined metric of temperature and precipitation changes under different strength of solar irradiation reduction. The Pareto improving, choosing the level of SRM that minimizes damages for all regions without making any region worse off (Moreno-Cruz et al., 2012), for temperature, precipitation and combined metric of temperature and precipitation also explored in Kravitz et al.(2014). We extend the work of Kravitz et al. (2014) by quantifying the regional inequalities and effectiveness represented by these two variables using the RCR method for each of the four GeoMIP experiments. Furthermore, our method of assessing the level of natural variability allows us to test the significance of regional inequalities and effectiveness in each experiment for each model as well as the significance of differences among different experiments.

Fig. 3. Ensemble mean of SAT anomalies for *G1 — piControl*, *abrupt4xCO2 — piControl*, *G2 — piControl*, *1pctCO2 — piControl*, *G3 — rcp45_2010_2029*, *G4 — rcp45_2010_2029*, and *rcp45_2030_2069 — rcp45_2010_2029*. For *G1 — piControl* and *abrupt4xCO2 — piControl*, stippling indicates where fewer than 10/13 models agreed on the sign of change; fewer than 9/12 models agreed for *G2 — piControl* and *1pctCO2 — piControl;* fewer than 6/8 models agreed for *rcp45_2030_2069 — rcp45_2010_2029;* fewer than 2/3 models agreed for *G3 — rcp45_2010_2029;* fewer than 5/7 models agreed for *G4 — rcp45_2010_2029*.

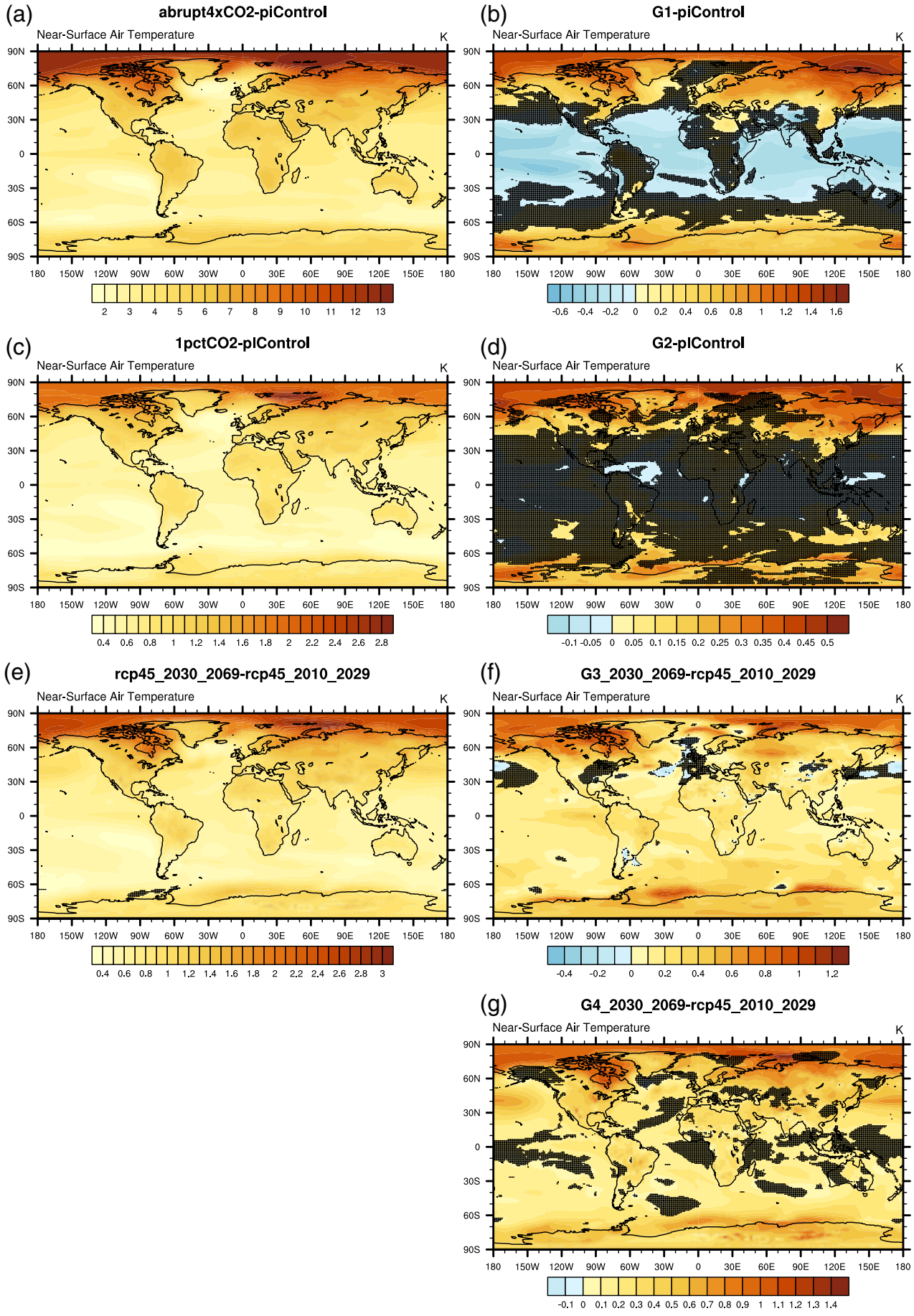
(a)
abrupt4xCO2-piControl
Near-Surface Air Temperature
K
90N 60N 30N 0 30S 60S 90S
180 150W 120W 90W 60W 30W 0 30E 60E 90E 120E 150E 180
2 3 4 5 6 7 8 9 10 11 12 13
(b)
G1-piControl
Near-Surface Air Temperature
K
-0.6 -0.4 -0.2 0 0.2 0.4 0.6 0.8 1 1.2 1.4 1.6
(c)
1pctCO2-piControl
Near-Surface Air Temperature
K
0.4 0.6 0.8 1 1.2 1.4 1.6 1.8 2 2.2 2.4 2.6 2.8
(d)
G2-piControl
Near-Surface Air Temperature
K
-0.1 -0.05 0 0.05 0.1 0.15 0.2 0.25 0.3 0.35 0.4 0.45 0.5
(e)
rcp45_2030_2069-rcp45_2010_2029
Near-Surface Air Temperature
K
0.4 0.6 0.8 1 1.2 1.4 1.6 1.8 2 2.2 2.4 2.6 2.8 3
(f)
G3_2030_2069-rcp45_2010_2029
Near-Surface Air Temperature
K
-0.4 -0.2 0 0.2 0.4 0.6 0.8 1 1.2
(g)
G4_2030_2069-rcp45_2010_2029
Near-Surface Air Temperature
K
-0.1 0 0.1 0.2 0.3 0.4 0.5 0.6 0.7 0.8 0.9 1 1.1 1.2 1.3 1.4

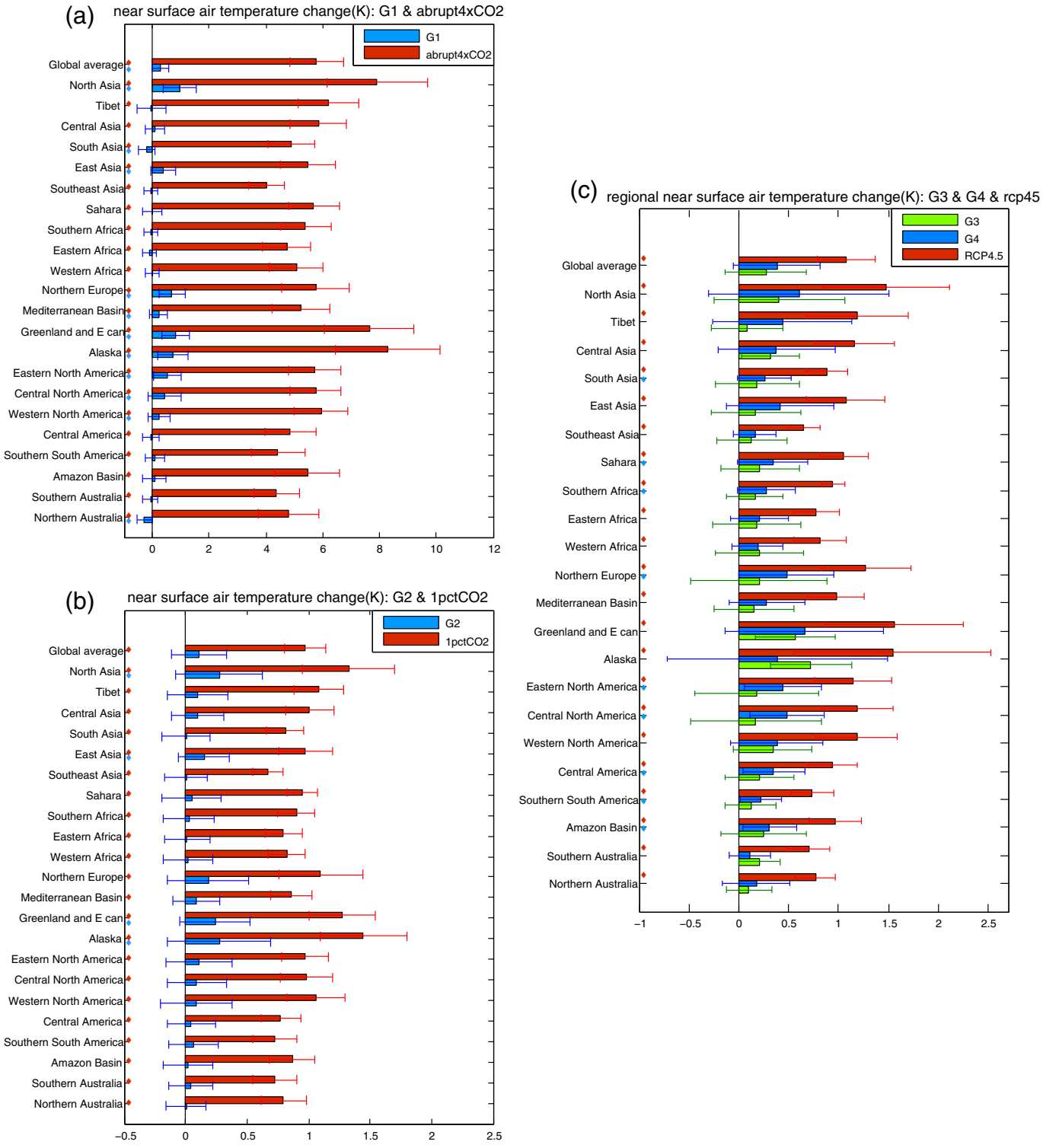

Fig. 4. Ensemble mean and standard deviation of area-weighted near surface air temperature for 22 regional anomalies in *G1 — piControl*, *abrupt4xCO2 — piControl*, *G2 — piControl*, *1pctCO2 — piControl*, *G3 — rcp45_2010_2029*, *rcp45_2030_2069 — rcp45_2010_2029*, and *G4 — rcp45_2010_2029*. Diamonds indicate the regional anomalies passed a Student's t test at the significance level of 0.05.

3. Results

3.1. Global and regional SAT changes

Figs. 3 and 4 show the multi-model ensemble mean of the SAT change at the grid and regional scales under different experiments. For GISS-E2-R, the global mean temperature and precipitation under *G3* and *rcp45* are very similar to each other (SI Fig. 1). There is no sign of change in global climate after sulfate aerosol has been injected, possibly due to the efficacy of SO_2 forcing in GISS-E2-R being relatively small as compared to CO_2 forcing. Therefore, the temperature and precipitation data from this model are not included in the *G3* study.

The SAT under *abrupt4xCO2* are obviously increased compared with *piControl* (Fig. 3a). The global average SAT increased 4.30 ± 0.75 °C (Table 2); these values are similar to those in previous studies (Schmidt et al., 2012; Good et al., 2013; Kravitz et al., 2013a). All the

Table 2
Ensemble mean and standard deviation of global average of SAT and precipitation change for *G1 — piControl*, *abrupt4xCO2 — piControl*, *G2 — piControl*, *1pctCO2 — piControl*, *G3 — rcp45_2010_2029*, *G4 — rcp45_2010_2029*, *rcp45_2030_69 — rcp45_2010_2029*.

Experiment	ΔT (°C)	ΔP (mm day^{-1})
G1 — piControl	0.05 ± 0.25	−0.128 ± 0.043
abrupt4xCO2 — piControl	4.30 ± 0.75	0.152 ± 0.055
G2 — piControl	0.07 ± 0.20	−0.020 ± 0.010
1pctCO2 — piControl	0.71 ± 0.15	0.023 ± 0.006
G3 — rcp45_2010_2029	0.23 ± 0.28	0.000 ± 0.019
G4 — rcp45_2010_2029	0.28 ± 0.31	0.001 ± 0.025
rcp45_2030_2069 — rcp45_2010_2029	0.81 ± 0.21	0.043 ± 0.018

regional scale SATs (Fig. 4a) show a statistically significant increase (95% significance level, see Section 2.2; the same significance level for regional change is used throughout this paper). *G1* successfully addresses the substantial global mean warming under *abrupt4xCO2*, restoring the global average SAT to its pre-industrial level (Table 2), but with relative warming over polar regions and cooling over the tropics (Fig. 3b). Previous studies (e.g., Govindasamy and Caldeira, 2000; Schmidt et al., 2012; Kravitz et al., 2013a) attribute the main reason for this SAT change pattern to the balancing of longwave greenhouse gas forcing by seasonally and latitudinally varying shortwave forcing. The regional scale land ensemble mean SAT change ranges from −0.28 °C to 0.96 °C (Fig. 4a).

SAT change under *1pctCO2* is much smaller but similar in spatial pattern to *abrupt4xCO2* (Fig. 3c). *G2* SAT change also has similar patterns to change under *G1* but with smaller magnitude and lower model agreement (Fig. 3d). This is likely due to the similar global radiative forcing spatial patterns between *G1* and *G2*. Regional scale land ensemble mean SAT change is between 0.00 °C and 0.27 °C (Fig. 4b). The SATs are significantly increased over much of the northern mid- and high-latitude land areas, but no regional scale SAT ensemble mean is larger than the corresponding across-model variation (defined as the multi-model ensemble standard deviation here and throughout this paper).

Over the period from 2030 to 2069, the global average SAT under *rcp45* increased by 0.81 ± 0.21 °C compared with the baseline (average over 2010–2029 under *rcp45*; Table 2). Additionally, all regional land SATs are significantly increased by 0.65 °C to 1.56 °C.

Under *G3*, the global mean SAT moderately increases by 0.23 ± 0.28 °C (Table 2) relative to the baseline. In contrast with *G1* and *G2*, under which the SAT decreased generally over low latitude oceans, the SAT decrease areas under *G3* are far fewer and more dispersed, mainly over mid and high latitudes such as central Asia, north Atlantic Ocean, northwest Australia, north Pacific Ocean and around Antarctica. At regional scales, the ensemble mean land SAT changes range from 0.08 °C to 0.72 °C. However, none of the regional changes are significant because of the small number of models in the *G3* ensemble and the large across-model variation.

For the geoengineering scenario *G4*, the 40 year annual global mean SAT increased by 0.28 ± 0.31 °C (Table 2). This is a slightly higher rise than under *G3*. The regional scale SAT increases range between 0.11 °C and 0.66 °C. The SATs in 9 regions are significantly increased under *G4*. All the regional land SAT ensemble means under *G4* increased relative to the baseline, and most regions have larger increases than under *G3*. This illustrates that the greenhouse gas induced radiative forcing in *rcp45* dominates that from 5 Tg a^{-1} SO_2 stratospheric injection over the 2030 to 2069 period.

3.2. Global and regional precipitation change

Figs. 5 and 6 show precipitation changes at the grid scale and regional scale, respectively. The global average precipitation increases by 0.15 ± 0.06 mm day^{-1} under *abrupt4xCO2* (Table 2 and Fig. 5a). Precipitation is strongly and robustly (at least ten of thirteen models agree on the sign of the change) increased over high latitude regions and the equatorial ocean. Precipitation robustly decreases under the sinking part of the Hadley Cell. These change patterns were also found by Schmidt et al. (2012) and Kravitz et al. (2013a).

Globally averaged precipitation under *G1* is decreased by −0.13 ± 0.04 mm day^{-1} (Table 2). The largest precipitation decrease occurs over equatorial parts of the Pacific Ocean. The multi-model mean precipitation in 19 regions is decreased under *G1*; changes in 16 of those regions are statistically significant (Fig. 6a). The patterns and global average of precipitation changes under *G1* are consistent with those discussed by Schmidt et al. (2012) and Kravitz et al. (2013a). A reduction in solar radiation imposed upon *abrupt4xCO_2* causes an initial suppression in precipitation. This suppression is sustained throughout experiment *G1* because of the lack of a slow response, primarily because the strongest feedbacks are related to global mean temperature changes, which are small (Kravitz et al., 2013b). From an energetic perspective, the suppression in precipitation under *G1* is primarily a result of the decrease of evaporative flux from the surface to the atmosphere (Kravitz et al., 2013b). Evaporative flux decreases are in part caused by an increase in atmospheric stability due to reduced insolation having a greater cooling effect on the surface than the mid-troposphere (Bala et al., 2008; Kravitz et al., 2013a). Evaporation decreases are also due to the CO_2 physiological effect, whereby plants close their stomata under high CO_2 conditions, reducing evapotranspiration over land (Fyfe et al., 2013; Kravitz et al., 2013b; Tilmes et al., 2013).

Precipitation changes under *1pctCO2* have weaker magnitudes than under *abrupt4xCO2* while exhibiting similar spatial patterns. Under *G2*, the precipitation pattern is also similar to that under *G1*, which may due to the similarity of the patterns of radiative forcing, but with a smaller magnitude of change and lower model agreement. Only 5 of the 22 regions show statistically significant changes in precipitation under *G2*.

Globally averaged precipitation under *rcp45* between 2030 and 2069 is moderately increased by 0.04 ± 0.02 mm day^{-1} compared with the baseline. The patterns of precipitation change under *rcp45* are similar to those under *abrupt4xCO2* and *1pctCO2*. Regional-scale land precipitation changes range from −0.07 to 0.14 mm day^{-1}. The ensemble mean precipitation is increased in 18 regions, and in 9 of those regions, the precipitation changes are statistically significant. The Amazon Basin has the largest across-model precipitation change variation.

The ensemble mean of the global average precipitation change under *G3* is negligible relative to the baseline, and the across-model variation (0.02 mm day^{-1}) is much larger than the ensemble mean. No regional change in any land region is significant.

Under *G4*, the ensemble mean of the global average precipitation change is also negligibly small with large across-model variation. The ranges of change of regional scale precipitation under *G4* overlap closely with those under *rcp45*. Precipitation is significantly increased over East Asia and significantly decreased over the Amazon Basin under *G4*.

3.3. Effectiveness and related regional inequalities of different SRM scenarios

Fig. 7 shows the regional inequality, and Fig. 8 the actual effectiveness (line and point) and corresponding noise (box) of individual models for scenarios *G1* to *G4* for temperature and precipitation. *G1* has low noise in regional inequality of temperature (0.6°–1.1°; Fig. 7), while the noise is larger for *G3* and *G4* (3.4°–8.6°) and larger again for *G2* (3.5°–11.7°). Note that similar regional inequalities between different models do not necessarily mean that the regional changes of these models are similar, as regional inequality depends on the temperature or precipitation changes in 22 regions under both the SRM scenario and the corresponding elevated CO_2 scenario. Regional inequality noise in precipitation (*G1*: 4.0°–8.0°. *G2*: 21.8°–37.6°, *G3* and *G4*: 13.2°–42.6°) is larger than for temperature. The regional inequality of temperature for all models under *G1*, *G3*, and *G4* is statistically significant (defined as being larger than their corresponding noise levels; we

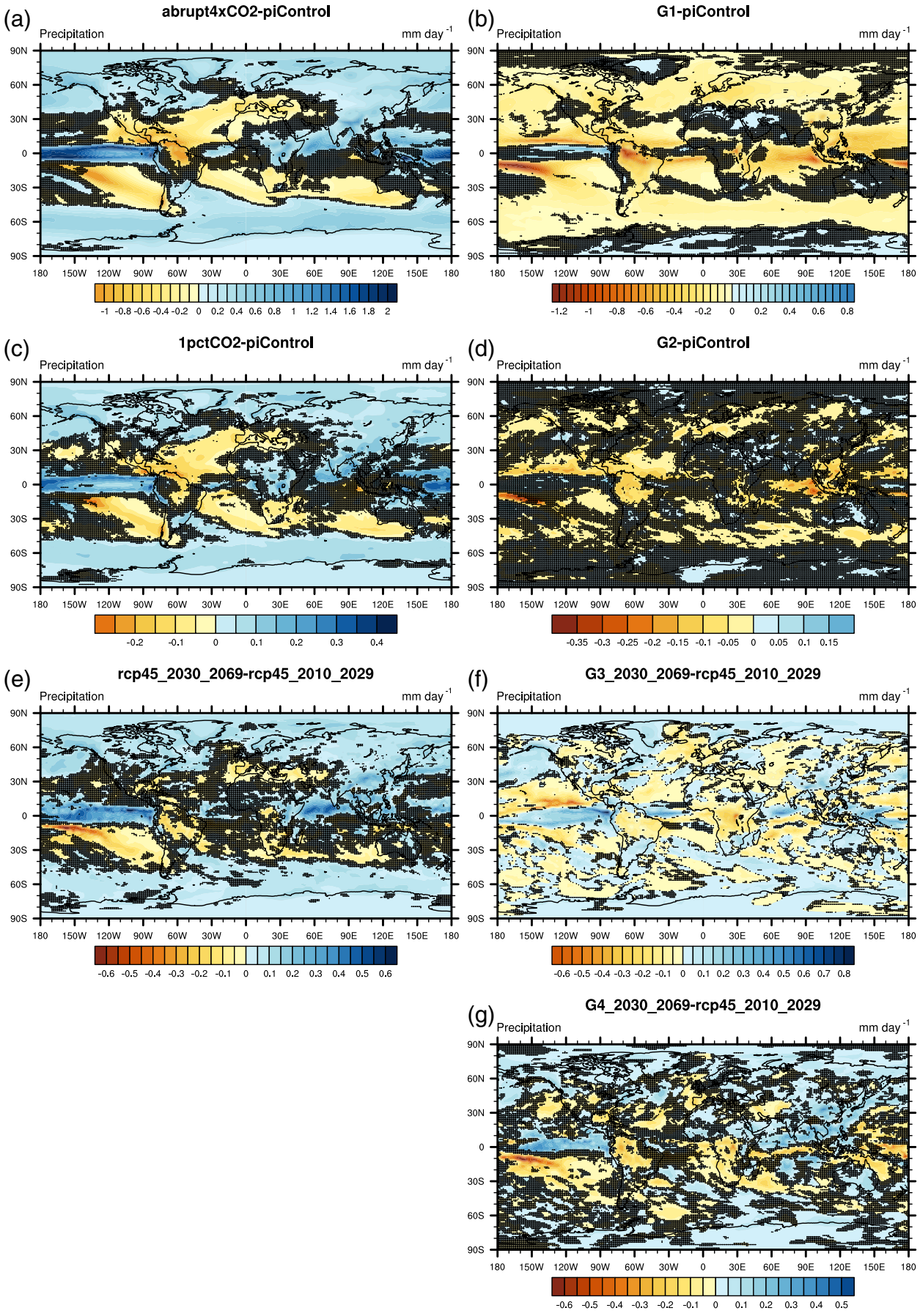

Fig. 5. The same as that for Fig. 3 but for precipitation anomalies.

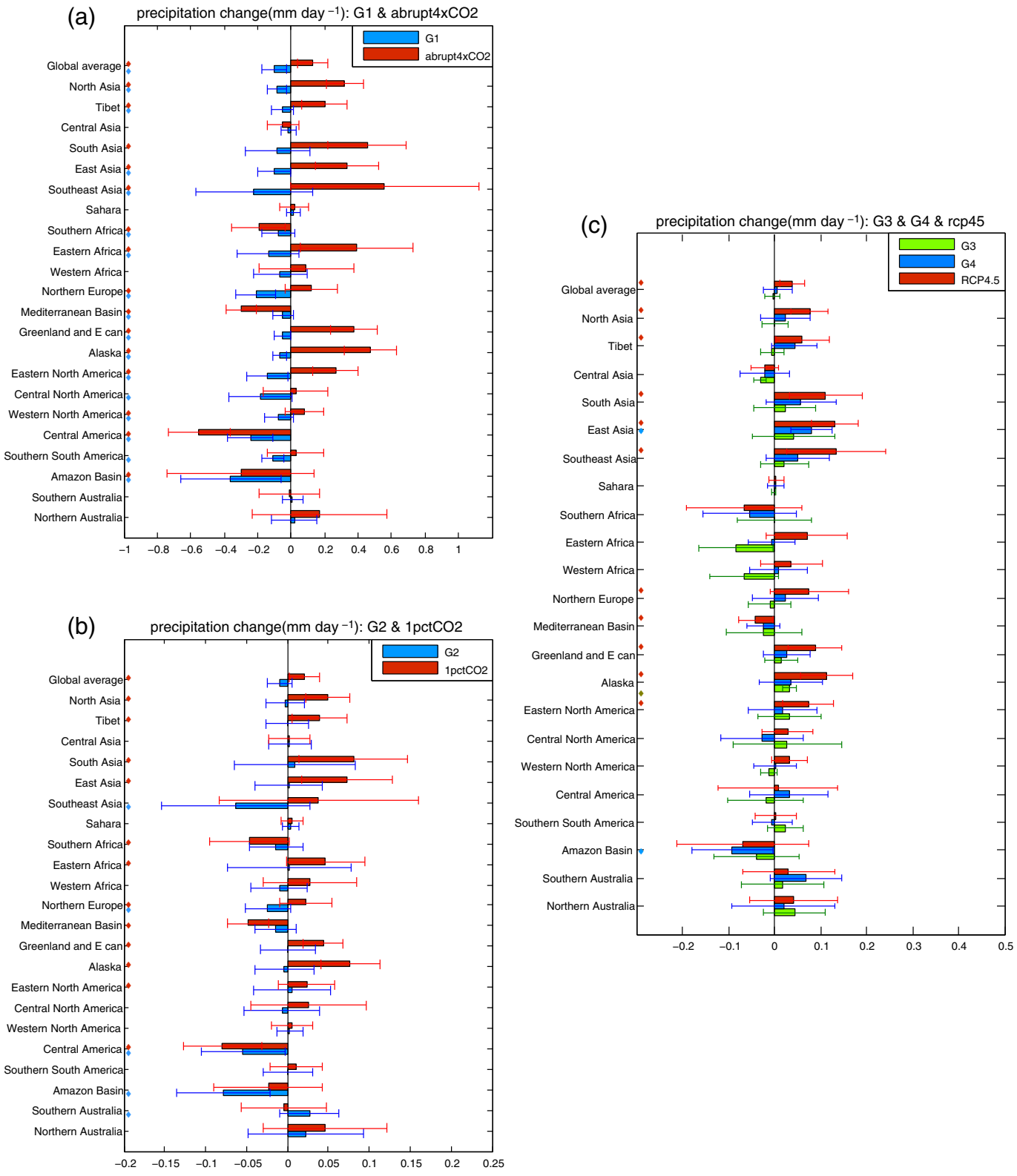

Fig. 6. The same as that for Fig. 4 but for precipitation regional anomalies.

use this definition in the remainder of this paper). For *G2*, 5 of 11 models have a regional inequality of temperature that is significantly different from noise. The regional inequalities of precipitation for all *G1* and *G3* models, as well as 6 of 7 *G4* models, are significantly different from their corresponding noise levels. For *G2*, the regional inequality of precipitation is significantly different from noise in 6 of 11 models. *G4* has the largest regional inequality across-model variations (multimodel ensemble standard deviation) for both temperature and precipitation.

Although temperature and precipitation inequalities of *G1* are smaller than *G2* for most of models, none of them are significant as none of the regional inequality differences between *G1* and *G2* are larger than corresponding noise in *G2* (Fig. 7). The temperature and precipitation

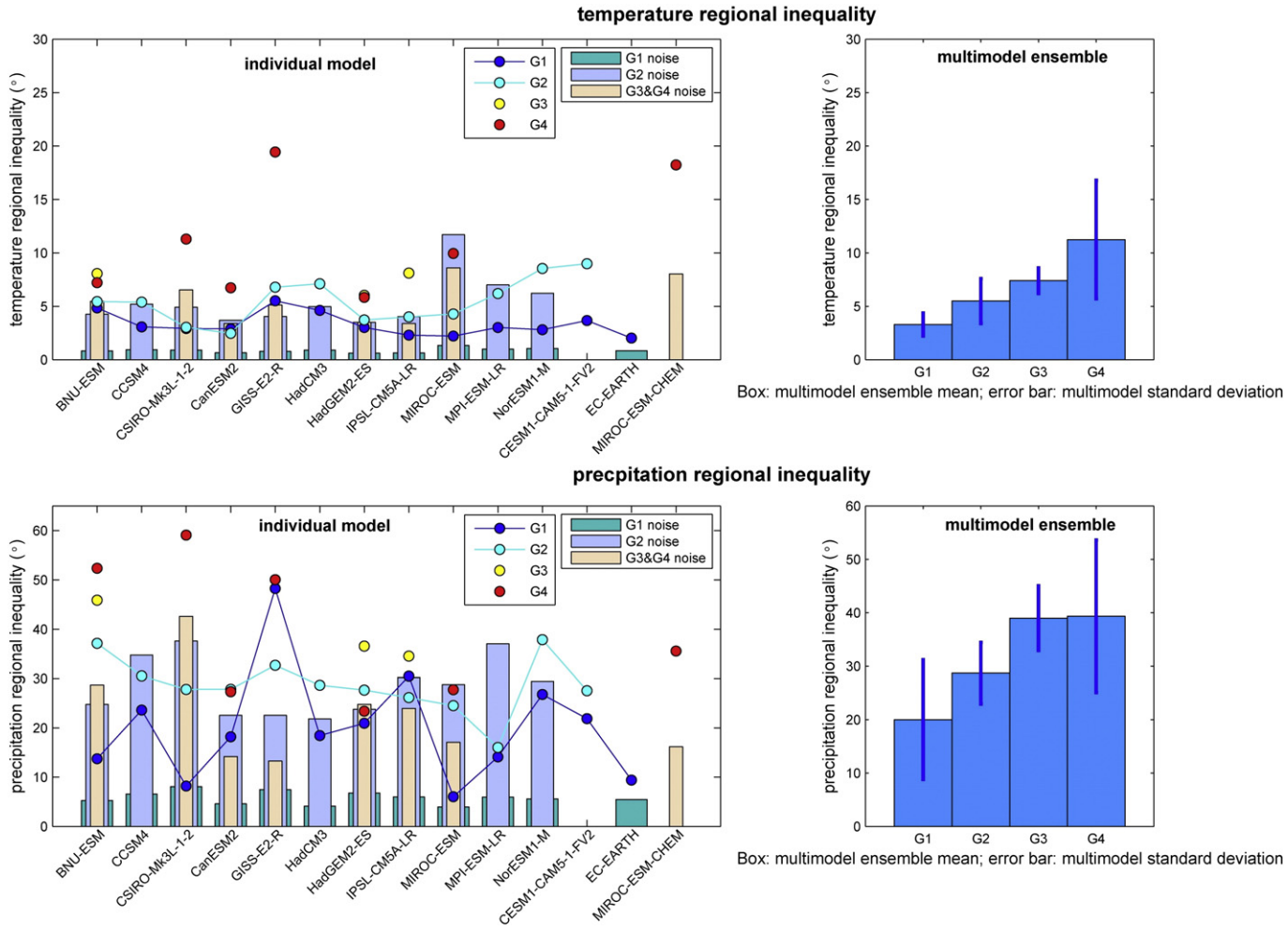

Fig. 7. Individual model, multi-model ensemble mean and standard deviation of regional inequality φ (°; Eq. (3)) of experiment *G1*, *G2*, *G3* and *G4* for near surface air temperature and precipitation. Calculated noise levels for *G3* and *G4* are the same for same model as both experiments used *rcp45* as the elevated CO_2e scenario. CESM-CAM5.1-FV was not included in the noise calculation for *G1* and *G2* as its *piControl* simulation only includes model 50 yrs.

regional inequality differences between *G3* and *G4* are not significant for 2 of 2 models that simulated both *G3* and *G4*. Most models under the solar dimming geoengineering scenarios (*G1* and *G2*) have temperature and precipitation regional inequalities smaller than under the SO_2 geoengineering scenarios (*G3* and *G4*), but no more than half of the models are significantly smaller.

Fig. 8 shows that for actual effectiveness of temperature, *G1* also has the smallest noise among the four experiments (0.01%–0.08%) and is the closest to 100% effective (98.7%–99.8%). The noise in actual effectiveness of temperature is 0.5%–5.6% for *G2* and 0.5%–3.0% for *G3* and *G4*. Under *G2*, 8 of 12 models are significantly different from the noise, and all models in *G3* and *G4* are significantly different from the noise. For actual effectiveness of precipitation, the noise in *G1* models is small (0.6%2.1%). *G2*, *G3* and *G4* have larger noise (*G2*: 19.7%–57.6%; *G3* and *G4*: 6.3–58.5%). Actual effectiveness of precipitation for *G1* to *G4* is significantly different from their corresponding noise for most models (*G1*: 12/12; *G2*: 6/11; *G3*: 3/3; *G4*: 6/7).

For 8 of 11 models that simulated both *G1* and *G2*, temperature actual effectiveness of *G1* is significantly higher than *G2* (Fig. 8). However, only 3 of 11 models' precipitation actual effectiveness of *G1* are significantly higher than *G2*. Temperature actual effectiveness of *G3* is significantly higher than that of *G4* for 2 of 2 models while none of models' precipitation actual effectiveness of *G3* is significantly higher than that of *G4*. More than half of the models under the solar dimming geoengineering scenarios (*G1* and *G2*) have temperature actual effectivenesses that are significantly higher than under the SO_2 geoengineering scenarios (*G3* and *G4*). For precipitation actual effectiveness, *G1* is significantly higher than for *G4* and *G2* and significantly higher than *G3* for more than half the models.

G1 has a large across model variation for precipitation regional inequality and actual effectiveness, with the differences between GISS-E2-R and the other models dominating (see Figs. 7 and 8).

The high compensation effectiveness, small regional inequality for SAT, and the lower compensation effectiveness with larger regional inequality for precipitation under *G1* are all consistent with the results of Moreno-Cruz et al. (2012), although Moreno-Cruz et al. (2012) only used one model. Previous studies also showed the difficulty of simultaneous perfect compensation of temperature and precipitation change by uniform SRM (e.g., Bala et al., 2008; Ricke et al., 2010; Moreno-Cruz et al., 2012; Kravitz et al., 2013a; Tilmes et al., 2013).

Optimal compensation effectiveness is higher than actual compensation effectiveness in all the four GeoMIP experiments (SI Fig. 2, Table 3). *G4* has the largest SAT and precipitation ensemble mean compensation effectiveness increase, changing from 80% to 95% and from 46% to 59%, respectively (Table 3). These effectiveness differences show that none of the four geoengineering experiments is at their highest potential to compensate for temperature and precipitation changes under the corresponding greenhouse gas forcing experiments.

The adjustment percentage of SRM-compensated change needed to achieve optimal compensation effectiveness (SI Fig. 3, Table 3) under *G1* and *G2* indicates that these two experiments should have weaker solar reduction to reach optimum precipitation compensation effectiveness. This is because the hydrological cycle is more sensitive to short wave

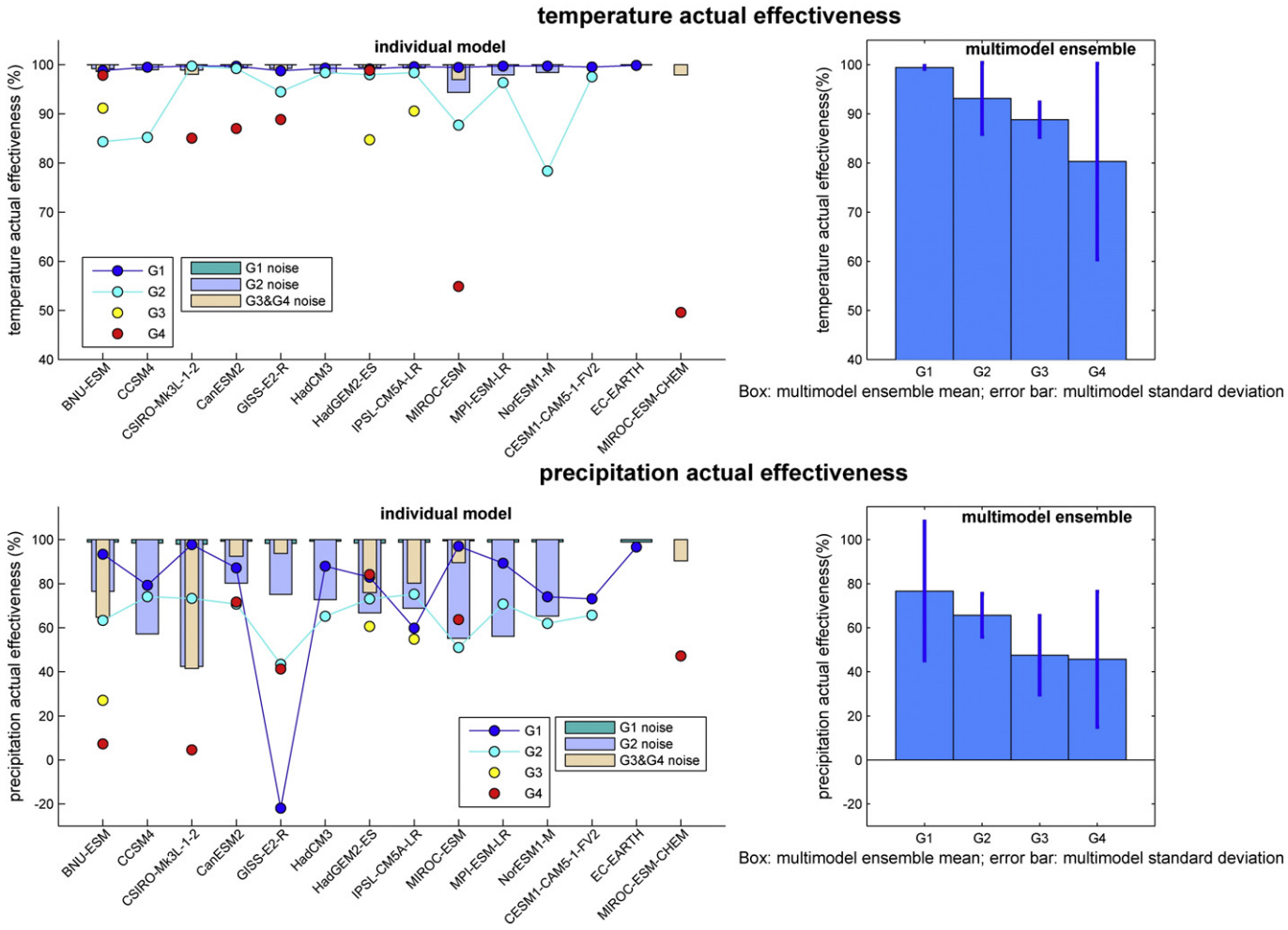

Fig. 8. The same as that for Fig. 7 but for actual compensation effectiveness (%; Eq. (7)).

surface warming than it is to greenhouse gas induced surface warming (e.g., Bala et al., 2008; Kleidon and Renner, 2013). Thus, although the cooling induced by solar irradiance reduction under *G1* and *G2* successfully counteracted the warming induced by CO_2 elevation, the resulting weakening of the hydrological cycle due to geoengineering is greater than the strengthening due to elevated CO_2. The adjustment percentage of SRM-compensated change under other experiments is not significant for precipitation in *G3* and *G4* and not significant for SAT in any experiment. The across-model variation of adjustment percentages to achieve optimal compensation effectiveness for SAT and precipitation is larger than the across-model variations in the other three metrics (regional inequality, actual compensation effectiveness and optimal compensation effectiveness) used in this study. This is because across-model variations in the other three metrics contribute to the across-model variation of the adjustment percentage. The adjustment percentage across-model variation for SAT and precipitation under *G3* and *G4* is larger than those under *G1* and *G2*.

4. Discussion and conclusions

In this study four GeoMIP experiments were analyzed using the results from up to 13 earth system models. We first investigated the robustness of global and regional SAT and precipitation change. We then explored the regional inequality, climate compensation effectiveness and adjustment percentage of SRM-compensated change needed to achieve optimal climate compensation effectiveness based on multi-model results.

Table 3
Multi-model ensemble mean and standard deviation of regional inequality φ (°; Eq. (3)), actual and optimal compensation effectiveness (%; Eqs. (7) and (8)) and adjustment percentage (%; Eq. (9)) of SRM compensated change under experiment *G1*, *G2*, *G3* and *G4* for near surface air temperature (T) and precipitation (P). All models available for each experiment in SI Table 1 are used. All the values in this table are the result of rounding original floating point value to nearest integer.

Experiment	Regional inequality φ (°)		Actual effectiveness (%)		Optimal effectiveness (%)		Adjustment percentage (%)	
	T	P	T	P	T	P	T	P
G1	3 ± 1	20 ± 11	99 ± 0	77 ± 32	100 ± 0	86 ± 14	1 ± 5	−18 ± 15
G2	6 ± 2	29 ± 6	93 ± 7	66 ± 10	99 ± 1	76 ± 8	14 ± 35	−20 ± 16
G3	8 ± 1	39 ± 6	86 ± 6	48 ± 18	98 ± 0	60 ± 10	31 ± 51	−13 ± 40
G4	11 ± 6	39 ± 14	80 ± 20	46 ± 31	95 ± 4	59 ± 23	71 ± 91	20 ± 62

As previous studies have shown (e.g., Jones et al., 2013; Kravitz et al., 2013a), under the idealized SRM experiments of *G1* and *G2*, the global average SATs are successfully restored close to pre-industrial levels, although with a relative tropical decrease and polar increase pattern. Here we quantify that the corresponding effectiveness, as measured by the RCR method, is quite high. However, these two experiments resulted in reduced global precipitation, thus their corresponding precipitation effectiveness is much smaller than those for SAT.

Among the four SRM scenarios, the regional inequalities of temperature and precipitation compensation for *G1*, *G3* and *G4* are significantly different from their corresponding noise levels for most of models. However, the regional inequalities of temperature and precipitation compensation for *G2* are not significantly different from the noise for most, and half of models respectively. This may be caused by the low signal to noise ratio in *G2*. The regional inequality and actual effectiveness differences among the four SRM scenarios for many models are not significant compared with the noise, especially for regional inequality. However, in more than half the models, temperature actual effectiveness under the solar dimming geoengineering scenarios (*G1* and *G2*) is significantly higher than that under the SO_2 geoengineering scenarios (*G3* and *G4*).

The difference between actual and optimal effectiveness supports earlier analysis (MacMartin et al., 2013) that balancing the TOA radiation budget does not produce equal regional responses. The optimum effectiveness can be reached by reducing or increasing the SRM, but the result depends on the choice of regions, the weighting given to each region, and the metric used to aggregate all regions; this was also deduced from the single-model experiments (Moreno-Cruz et al., 2012). Our multi-model analysis brings extra information on the sensitivity of these results to model physics. Cleary results differ depending on the model used, especially in the case of highly complex simulations such as SO_2 injections. This results in much across-model noise, but a reasonably robust conclusion that aerosol injection is less effective that solar dimming, and more likely to result in regional inequalities of climate response. Here we have assumed only globally uniform forcing from SRM. If non-uniform optimization is available, via spatial and temporal varying SRM, the regional inequality will certainly be different. Residual temperature and precipitation changes in the worst-off region (however that is defined), or the required solar reduction for the same residual climate change, may be reduced (MacMartin et al., 2013). The metrics we use here show, as expected, that precipitation is inherently more variable across different regions than temperature. The large across-model variation in the adjustment percentage of compensated SAT and precipitation change by SRM to achieve optimal compensation effectiveness sheds light on the uncertainty accumulation effect in optimizing compensation effectiveness of SRM.

While caution is needed to interpret the results based purely on the RCR methodology in this study, the findings are in broad agreement with other studies using different methods or considerably fewer models. The RCR methodology is a useful tool that aids in the visualization and comparison of multiple model climate fields across many regions in a simple set of metrics. The regions here are assumed equally weighted, but it is easy to adjust the weighting based on economic or population loadings as desired (e.g. Moreno-Cruz et al., 2012). Perhaps more fundamentally, we used (as have others) a simple quadratic damage function for climate change. In practice, such decisions are beyond the remit of the natural sciences and ultimately are decided by societal values. However, the inputs to the analysis come from earth system models and, therefore, are limited by the quality of the climate system representation in those models. Although the four SRM experiments in GeoMIP represent far from real-world implementations of the SRM, the robust features and contrasting areas of doubt are becoming clearer. To move towards potentially more useful regional or seasonal geoengineering modeling requires advances, the identification of key region-specific damage functions, and better treatment of geoengineering methods in the earth system models.

Supplementary data to this article can be found online at http://dx.doi.org/10.1016/j.gloplacha.2015.02.010.

Acknowledgments

We thank Juan Moreno-Cruz, Hans-F Graf, and an anonymous reviewer for their comments. We thank all participants of the Geoengineering Model Intercomparison Project and their model development teams, CLIVAR/WCRP Working Group on Coupled Modeling for endorsing GeoMIP, and the scientists managing the Earth System Grid data nodes who have assisted with making GeoMIP output available. We acknowledge the World Climate Research Programme's Working Group on Coupled Modelling, which is responsible for CMIP, and we thank the climate modeling groups for producing and making available their model output. For CMIP the U.S. Department of Energy's Program for Climate Model Diagnosis and Intercomparison provides coordinating support and led the development of software infrastructure in partnership with the Global Organization for Earth System Science Portals. DJ, XY, XC and JCM thank all members of the BNU-ESM model group and support from the Joint Center for Global Change Studies (JCGCS), as well as the Center of Information and Network Technology at Beijing Normal University for assistance in publishing the GeoMIP dataset. Ben Kravitz is supported by the Fund for Innovative Climate and Energy Research (FICER). The Pacific Northwest National Laboratory is operated for the U.S. Department of Energy by Battelle Memorial Institute under contract DE-AC05-76RL01830. Simulations performed by Ben Kravitz were supported by the NASA High-End Computing (HEC) Program through the NASA Center for Climate Simulation (NCCS) at Goddard Space Flight Center.

References

Bala, G., Duffy, P.B., Taylor, K.E., 2008. Impact of geoengineering schemes on the global hydrological cycle. Proc. Natl. Acad. Sci. 105 (22), 7664–7669.
Ban-Weiss, G.A., Caldeira, K., 2010. Geoengineering as an optimization problem. Environ. Res. Lett. 5 (3).
Berdahl, M., Robock, A., Ji, D., Moore, J.C., Jones, A., Kravitz, B., Watanabe, S., 2014. Arctic Cryosphere Response in the Geoengineering Model Intercomparison Project (GeoMIP) G3 and G4 scenarios. J. Geophys. Res. Atmos. 119 (3), 1308–1321.
Budyko, M.I., 1977. Climatic Changes. American Geophysical Union, Washington D.C.
Caldeira, K., Keith, D.W., 2010. The need for climate engineering research. Issues Sci. Technol. 27 (1), 57–62.
Cline, W.R., 1992. The Economics of Global Warming. Institute of International Economics, Washington, DC.
Crutzen, P.J., 2006. Albedo enhancement by stratospheric sulfur injections: a contribution to resolve a policy dilemma? Clim. Chang. 77 (3–4), 211–219.
Fyfe, J.C., Cole, J.N.S., Arora, V.K., Scinocca, J.F., 2013. Biogeochemical carbon coupling influences global precipitation in geoengineering experiments. Geophys. Res. Lett. 40 (3), 651–655.
Giorgi, F., Francisco, R., 2000. Evaluating uncertainties in the prediction of regional climate change. Geophys. Res. Lett. 27 (9), 1295–1298.
Good, P., Gregory, J.M., Lowe, J.A., Andrews, T., 2013. Abrupt CO_2 experiments as tools for predicting and understanding CMIP5 representative concentration pathway projections. Clim. Dyn. 40 (3–4), 1041–1053.
Govindasamy, B., Caldeira, K., 2000. Geoengineering Earth's radiation balance to mitigate CO_2-induced climate change. Geophys. Res. Lett. 27 (14), 2141–2144.
Jones, A., Haywood, J., Boucher, O., Kravitz, B., Robock, A., 2010. Geoengineering by stratospheric SO_2 injection: results from the Met Office HadGEM(2) climate model and comparison with the Goddard Institute for Space Studies ModelE. Atmos. Chem. Phys. 10 (13), 5999–6006.
Jones, A., Haywood, J.M., Alterskjaer, K., Boucher, O., Cole, J.N.S., Curry, C.L., Irvine, P.J., Ji, D., Kravitz, B., Kristjánsson, J.E., Moore, J.C., Niemeier, U., Robock, A., Schmidt, H., Singh, B., Tilmes, S., Watanabe, S., Yoon, J.-H., 2013. The impact of abrupt suspension of solar radiation management (termination effect) in experiment G2 of the Geoengineering Model Intercomparison Project (GeoMIP). J. Geophys. Res. Atmos. 118 (17), 9743–9752.
Kleidon, A., Renner, M., 2013. A simple explanation for the sensitivity of the hydrologic cycle to surface temperature and solar radiation and its implications for global climate change. Earth Syst. Dyn. 4 (2), 455–465.
Kravitz, B., Robock, A., Boucher, O., Schmidt, H., Taylor, K.E., Stenchikov, G., Schulz, M., 2011. The Geoengineering Model Intercomparison Project (GeoMIP). Atmos. Sci. Lett. 12 (2), 162–167.
Kravitz, B., Caldeira, K., Boucher, O., Robock, A., Rasch, P.J., Alterskjær, K., Karam, D.B., Cole, J.N.S., Curry, C.L., Haywood, J.M., Irvine, P.J., Ji, D., Jones, A., Kristjánsson, J.E., Lunt, D.J.,

Moore, J.C., Niemeier, U., Schmidt, H., Schulz, M., Singh, B., Tilmes, S., Watanabe, S., Yang, S., Yoon, J.-H., 2013a. Climate model response from the Geoengineering Model Intercomparison Project (GeoMIP). J. Geophys. Res. Atmos. 118 (15), 8320–8332.

Kravitz, B., Rasch, P.J., Forster, P.M., Andrews, T., Cole, J.N.S., Irvine, P.J., Ji, D., Kristjánsson, J.E., Moore, J.C., Muri, H., Niemeier, U., Robock, A., Singh, B., Tilmes, S., Watanabe, S., Yoon, J.-H., 2013b. An energetic perspective on hydrological cycle changes in the Geoengineering Model Intercomparison Project. J. Geophys. Res. Atmos. 118 (23), 13,087–13,102.

Kravitz, B., MacMartin, D.G., Robock, A., Rasch, P.J., Ricke, K.L., Cole, J.N.S., Curry, C.L., Irvine, P.J., Ji, D., Keith, D.W., Kristjánsson, J.E., Moore, J.C., Muri, H., Singh, B., Tilmes, S., Watanabe, S., Yang, S., Yoon, J.-H., 2014. A multi-model assessment of regional climate disparities caused by solar geoengineering. Environ. Res. Lett. 9 (7), 074013.

Latham, J., 1990. Control of global warming? Nature 347 (6291), 339–340.

MacCracken, M.C., Shin, H.J., Caldeira, K., Ban-Weiss, G.A., 2012. Climate response to imposed solar radiation reductions in high latitudes. Earth Syst. Dyn. Discuss. 3 (2), 715–757.

MacMartin, D.G., Keith, D.W., Kravitz, B., Caldeira, K., 2013. Management of trade-offs in geoengineering through optimal choice of non-uniform radiative forcing. Nat. Clim. Chang. 3 (4), 365–368.

Manne, A., Mendelsohn, R., Richels, R., 1995. MERGE: a model for evaluating regional and global effects of GHG reduction policies. Energy Policy 23 (1), 17–34.

Mautner, M., 1989. Deep-space solar screens against climatic warming: technical and research requirements. Space Utilization and Applications in the Pacific, Proceedings of the Third Pacific Basin International Symposium on Advances in Space Science, Technology and Applications. American Astronautical Society, Los Angeles, p. 711.

Moore, J.C., Rinke, A., Yu, X., Ji, D., Cui, X., Li, Y., Alterskjær, K., Kristjánsson, J.E., Muri, H., Boucher, O., Huneeus, N., Kravitz, B., Robock, A., Niemeier, U., Schulz, M., Tilmes, S., Watanabe, S., Yang, S., 2014. Arctic sea ice and atmospheric circulation under the GeoMIP G1 scenario. J. Geophys. Res. Atmos. 119 (2), 567–583.

Moreno-Cruz, J.B., Ricke, K., Keith, D., 2012. A simple model to account for regional inequalities in the effectiveness of solar radiation management. Clim. Chang. 110 (3–4), 649–668.

Peck, S.C., Teisberg, T.J., 1992. CETA: a model for carbon emissions trajectory assessment. Energy J. 13 (1), 55–78.

Peck, S.C., Teisberg, T.J., 1994. Optimal carbon emissions trajectories when damages depend on the rate or level of global warming. Clim. Chang. 28 (3), 289–314.

Rasch, P.J., Tilmes, S., Turco, R.P., Robock, A., Oman, L., Chen, C.C., Stenchikov, G.L., Garcia, R.R., 2008. An overview of geoengineering of climate using stratospheric sulphate aerosols. Philos. Transact. A Math. Phys. Eng. Sci. 366 (1882), 4007–4037.

Ricke, K.L., Morgan, G., Allen, M.R., 2010. Regional climate response to solar-radiation management. Nat. Geosci. 3 (8), 537–541.

Ricke, K.L., Moreno-Cruz, J.B., Caldeira, K., 2013. Strategic incentives for climate geoengineering coalitions to exclude broad participation. Environ. Res. Lett. 8 (1), 014021.

Schmidt, H., Alterskjær, K., Bou Karam, D., Boucher, O., Jones, A., Kristjánsson, J.E., Niemeier, U., Schulz, M., Aaheim, A., Benduhn, F., Lawrence, M., Timmreck, C., 2012. Solar irradiance reduction to counteract radiative forcing from a quadrupling of CO_2: climate responses simulated by four earth system models. Earth Syst. Dyn. 3 (1), 63–78.

Shepherd, J., et al., 2009. Geoengineering the Climate: Science, Governance and Uncertainty. Royal Society, London.

Taylor, K.E., Stouffer, R.J., Meehl, G.A., 2012. An overview of CMIP5 and the experiment design. Bull. Am. Meteorol. Soc. 93 (4), 485–498.

Tilmes, S., Fasullo, J., Lamarque, J.-F., Marsh, D.R., Mills, M., Alterskjær, K., Muri, H., Kristjánsson, J.E., Boucher, O., Schulz, M., Cole, J.N.S., Curry, C.L., Jones, A., Haywood, J., Irvine, P.J., Ji, D., Moore, J.C., Karam, D.B., Kravitz, B., Rasch, P.J., Singh, B., Yoon, J.-H., Niemeier, U., Schmidt, H., Robock, A., Yang, S., Watanabe, S., 2013. The hydrological impact of geoengineering in the Geoengineering Model Intercomparison Project (GeoMIP). J. Geophys. Res. Atmos. 118 (19), 11,036–11,058.

Wigley, T.M.L., 2006. A combined mitigation/geoengineering approach to climate stabilization. Science 314 (5798), 452–454.